International Journal of Coal Geology 121 (2014) 44–52

Contents lists available at ScienceDirect

International Journal of Coal Geology

journal homepage: www.elsevier.com/locate/ijcoalgeo

# A dynamic prediction model for gas–water effective permeability based on coalbed methane production data

H. Xu *, D.Z. Tang, S.H. Tang, J.L. Zhao, Y.J. Meng, S. Tao

*School of Energy Resources, China University of Geosciences, Beijing 100083, PR China*
*Coal Reservoir Laboratory of National Engineering Research Center of Coalbed Methane Development & Utilization, Beijing 100083, PR China*

ARTICLE INFO

*Article history:*
Received 17 July 2013
Received in revised form 18 November 2013
Accepted 20 November 2013
Available online 28 November 2013

*Keywords:*
Coal reservoir
Effective permeability
Relative permeability
Prediction model
Qinshui basin

ABSTRACT

An understanding of the relative permeability of gas and water in coal reservoirs is vital for coalbed methane (CBM) development. In this work, a prediction model for gas–water effective permeability is established to describe the permeability variation within coal reservoirs during production. The effective stress and matrix shrinkage effects are taken into account by introducing the Palmer and Mansoori (PM) absolute permeability model. The endpoint relative permeability is calibrated through experimentation instead of through the conventional Corey relative permeability model, which is traditionally employed for the simulation of petroleum reservoirs. In this framework, the absolute permeability model and the relative permeability model are comprehensively coupled under the same reservoir pressure and water saturation conditions through the material balance equation. Using the Qinshui Basin as an example, the differences between the actual curve that is measured with the steady-state method and the simulation curve are compared. The model indicates that the effective permeability is expressed as a function of reservoir pressure and that the curve shape is controlled by the production data. The results illustrate that the PM–Corey dynamic prediction model can accurately reflect the positive and negative effects of coal reservoirs. In particular, the model predicts the matrix shrinkage effect, which is important because it can improve the effective permeability of gas production and render the process more economically feasible.


## 1. Introduction

At present, China is the largest consumer and producer of coal in the world (Dai et al., 2012). According to the World Energy Council, as of 2009, China contained an estimated 103.87 Gt of recoverable coal reserves, comprising 14% of the world's total reserves. This is the third largest coal reserve, behind those of the United States and Russia. Coal comprised approximately 74% of China's total primary energy consumption, and approximately 60% of chemical materials are derived from coal products (Dai et al., 2012).

In recent years, the commercial development of coalbed methane (CBM) in high-rank coal reservoirs of the Qinshui basin in China has achieved significant success (Cai et al., 2011; Lv et al., 2012; Xu et al., 2012). However, the breakthroughs in the coalbed methane industry have been accompanied by a number of difficulties. The permeability of coal reservoirs and the associated implications are a concern in the evaluation of coalbed methane development (Palmer, 2009; Pan and Connell, 2012; Sparks et al., 1995; Xu et al., 2005). Coalbed methane development usually occurs in three stages: water single-phase flow, gas and water two-phase flow, and gas single-phase flow (Ates and Barron, 1998; Chen et al., 2009). The gas production rate strongly depends on the relative permeabilities of gas and water (Ham and Kantzas, 2008). Relative permeability is an indispensable parameter in simulations of CBM production (Shi et al., 2008).

During the CBM production process, the physical parameters of the coal reservoir change dynamically due to effective stress and matrix shrinkage effects (Pan et al., 2010). As the reservoir pressure decreases, the effective stress increases, and the porosity and absolute permeability decrease; however, these impacts are often counterbalanced by the coal matrix shrinkage effect, which increases the porosity and absolute permeability from the critical desorption pressure to the abandonment pressure (Chen et al., 2013). If the critical desorption pressure is higher, then the wells are more economical (Bustin, 1997; Cui and Bustin, 2005; McKee et al., 1988; Moore, 2012; Tao et al., 2012; Wang, 2006; Wang and Ward, 2009). The variations of matrix porosity can induce changes in the irreducible water saturation and affect not only the range of water saturation variation (Chen et al., 2013) but also the relative permeability. Therefore, these positive (coal matrix shrinkage) and negative (effective stress) effects are the key factors underlying the relative permeability curve during production. Considering these contrasting effects, an effective permeability model should couple the absolute permeability with the relative permeability under the same reservoir conditions. Such a model is important for the accurate quantification of the permeability variation in coal reservoirs during CBM production.

Presently, the most widely used methods for measuring the relative permeabilities of gas and water in the laboratory are the steady-state

* Corresponding author at: School of Energy Resources, China University of Geosciences, Beijing 100083, PR China. Tel.: +86 10 82320106; fax: +86 10 82326850.
*E-mail address:* Xuhao600@163.com (H. Xu).

0166-5162/$ – see front matter © 2013 Elsevier B.V. All rights reserved.
http://dx.doi.org/10.1016/j.coal.2013.11.008

(Hyman et al., 1992; Jones et al., 1988; Shen et al., 2011) and the unsteady-state (Paterson et al., 1992; Puri et al., 1991) methods, both of which are conventional methods for testing oil and gas. However, the theoretical basis of these testing methods may be unsuitable for the particular characteristics of coal reservoirs (Moore, 2012). Several indirect methods are available to assess the relative permeability curve, such as the use of production data (Clarkson et al., 2007, 2011) or log data (Conway et al., 1995) and the calculation of the capillary pressure curve (Brooks and Corey, 1966; Corey, 1954; Corey and Rathgens, 1956; Li, 2010; Pirson, 1958; Wyllie and Gardner, 1958; Zhou et al., 2007). However, these methods are primarily developed for conventional oil and gas reservoirs and result in significant errors when applied to coal reservoirs (Chen et al., 2013).

Here, the key factors that influence the effective permeability of gas and water are analyzed by considering the absolute permeability and relative permeability characteristics of coal reservoirs. Then, an average gas and water effective permeability dynamic prediction model is established using CBM production data and is compared to related experimental results for the Qinshui Basin.

## 2. Geological setting

The Qinshui Basin is situated in southeastern Shanxi province, China, with an area of $23.5 \times 10^3$ km$^2$ (Fig. 1). The basin is a large synclinorium with a bilateral symmetry. The main coal-bearing sequences occur in the Taiyuan and Shanxi Formations (Fig. 2). The total coal thickness of these formations is approximately 15 m. The Taiyuan Formation is approximately 50 to 135 m thick (generally less than 90 m) and consists of limestone, sandstone, siltstone, mudstone, and 14 coal seams. No. 15 coal is the main mineable coal seam, which has a thickness of 1 to 6 m over the entire area. The Shanxi Formation is 20 to 86 m thick and consists of sandstone, siltstone, mudstone, and 2 to 7 coal seams. The No. 3 seam is the main mineable coal seam, which has a thickness of 4 to 7 m over the entire area; it is the main target seam for CBM development in the southern Qinshui Basin (Lv et al., 2012).

## 3. Methods and experiments

To analyze the key factors that influence coal reservoir gas and water relative permeability, an absolute permeability model, which accounts for the positive and negative effects during production, and a relative permeability model, which is traditionally employed in numerical simulations, are coupled under the same reservoir pressure and water saturation conditions by applying the material balance equation with the production data. After calibrating the endpoint relative permeability, an average gas and water effective permeability dynamic prediction model is established to reflect the CBM development. Using the Qinshui Basin as an example, the differences between the experimentally measured curve and those curves estimated by the steady-state method and the simulation are compared.

### 3.1. Methods

In constructing the model, the following assumptions about the system are implemented: 1) the boundary is closed, and the radial flow of gas and water through the fracture system obeys Darcy's law; 2) the reservoir and the fluids are homogeneous, isotropic and homothermal during production; 3) primitive gas is adsorbed onto the inner surface of pores in the coal matrix; and 4) the gas is instantaneously desorbed from the matrix and immediately diffused to the fracture system at the critical desorption pressure.

The procedure to derive the relative permeability curves (i.e., the production data) in this work (Fig. 3) is detailed below:

1) The cumulative gas and water production data are obtained from actual production wells, and then the values for cumulative production are obtained at the two-phase seepage stage;
2) The reservoir pressure changes during the production process and estimated water saturation are simulated by the use of the material balance equations;
3) The absolute permeability changes are calculated by substituting the reservoir pressure into the absolute permeability model, and the

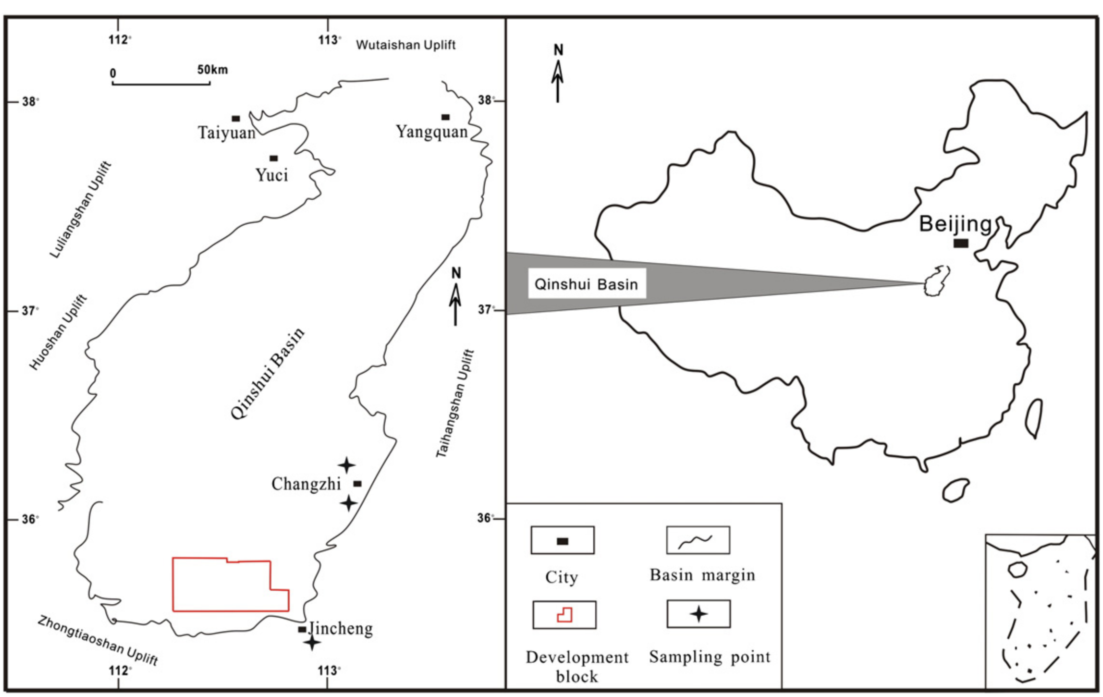


Fig. 1. Location of the Qinshui basin in China.

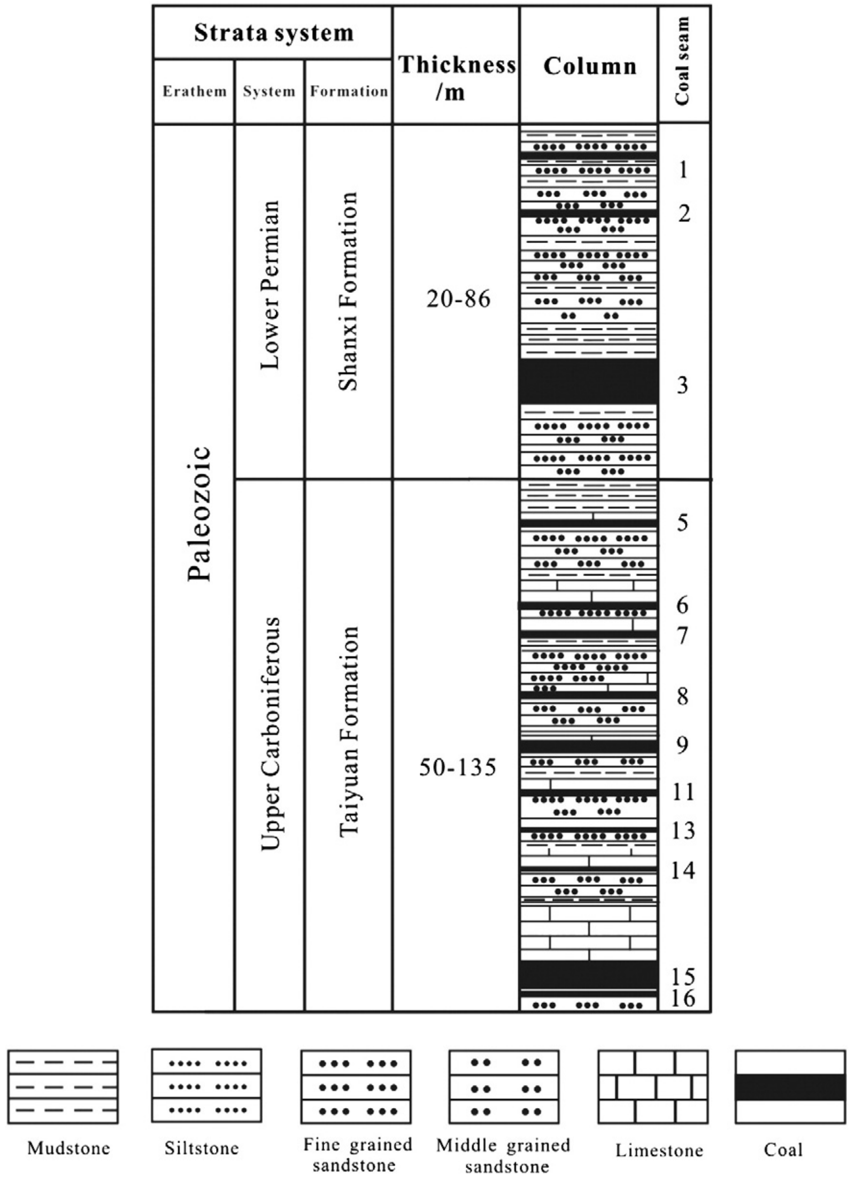


**Fig. 2.** Stratigraphic column showing coal-bearing formations in the Qinshui Basin.

relative permeability changes are computed by substituting the water saturation. The endpoint relative permeability is calibrated;

4) The calibrated relative permeability is coupled with the absolute permeability to obtain the effective permeability under the same reservoir conditions;
5) The curves of the gas and water effective permeabilities are plotted with effective permeability as the vertical coordinate and water saturation as the horizontal coordinate;
6) The efficiency of the dynamic prediction model is evaluated by comparing the simulated curve with the measured curve.

### 3.2. Experiments

Ten coal samples are collected directly from the working faces of underground mines in Qinshui Basin and are cut into 50 mm × 50 mm × 100 mm samples. Mean vitrinite reflectance (%$R_o$) measurements and maceral analyses (500 points) were performed on the same polished section of the coal samples using a Leitz MPV-3 photometer microscope, according to ISO 7404.3-1994 (1994) and ISO 7404.5-1994 (1994), respectively. Samples were analyzed for proximate analysis, including ash yield, moisture content and volatile matter, following Chinese national standard GB/T 212–2008 (2008) (Xu et al., 2012).

The gas–water relative permeability of each sample is then measured using the steady-state method. This experiment is based on the theory of one-dimensional Darcy flow and ignores the interactions of gravity and capillary pressure; it also assumes that the fluids are immiscible and incompressible. The gas and water effective permeability and relative permeability are calculated using Darcy's law. The endpoint relative permeability is also obtained through the experiments. The Palmer–Mansoori model and the material balance equation, which will be discussed later, mainly consider the cleat porosity. Therefore, this study uses the mercury injection method to obtain the fractal dimension of the coal samples and determine the relationship between irreducible water saturation and porosity. The mercury porosimetry experiments are performed using an Autopore III9420 instrument, which automatically registers pressure, pore radius, injection volume, and surface area. Volume injection curves are obtained for each sample at a pressure interval of 0.0074–7.35 MPa, corresponding to a pore radius range of 100 to 0.1 mm. Fractals and fractal geometry were used to describe highly disordered systems that are characterized by invariability with scale. Fractal systems are characterized by the fractal dimension.

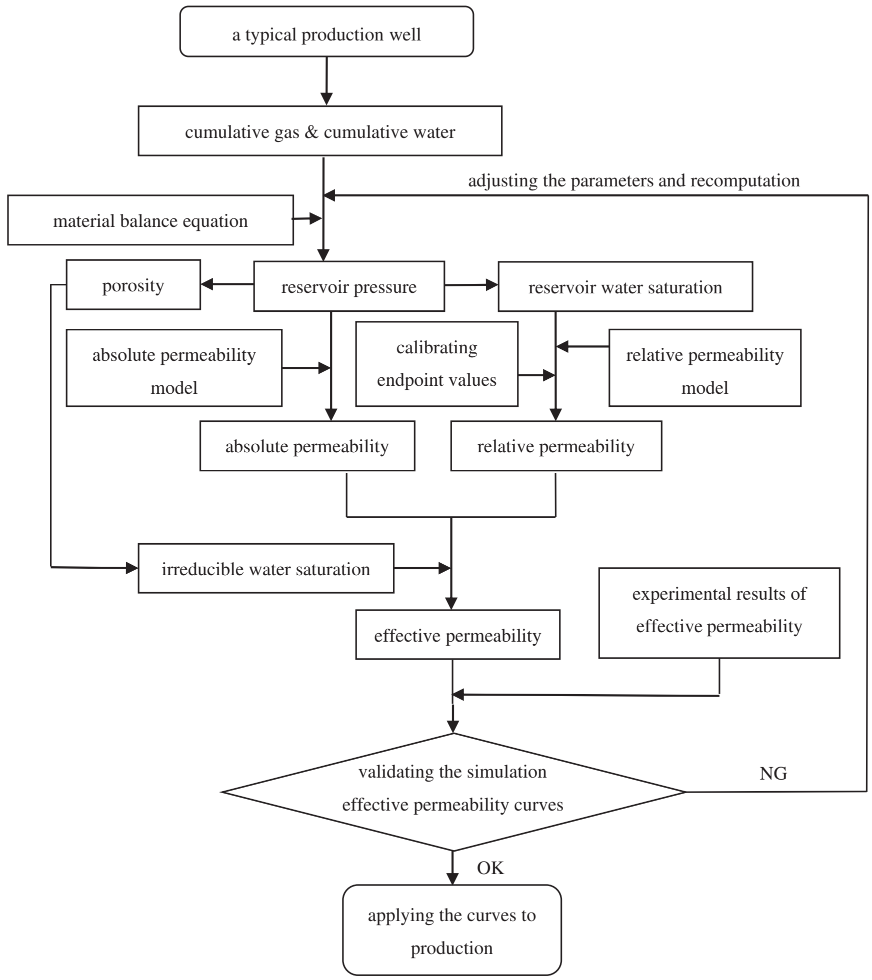


**Fig. 3.** Workflow used to generate relative permeability curves (OK represents acception, NG represents Next Generation).

The fractals of coals can be obtained from the mercury porosimetry analysis data (Friesen and Ogunsola, 1995; Fu et al., 2005; Mahamud et al., 2003). Mathematical models for fractal dimension analysis are provided by Friesen and Mikula (1987) and Yao et al. (2009).

Isothermal adsorption experiments are performed to obtain associated parameters, such as the Langmuir volume and Langmuir pressure at the Gas Research Center, Langfang Branch of Research Institute of Petroleum Exploration and Development. All of the coal samples are prepared by crushing and sieving them to a size of 0.18–0.25 mm (60–80 mesh), and then 100–125 g samples are weighed for the moisture equilibrium treatment. The moisture-equilibrium treatment for each sample is processed for at least four days. After these pretreatments, the coals are inserted into the sample cell of the IS-100 for the adsorption isotherm experiment. The experimental temperature and equilibrium pressure are 30 °C and up to 10 MPa, respectively.

## 4. Effective permeability model development for coal

### 4.1. Theoretical basis

Effective permeability, which is the ability of each phase to pass through a coal reservoir that is saturated by multiphase fluids, is the most directly relevant permeability parameter related to well production because it determines the final rate of gas production. Absolute permeability and irreducible water saturation change dynamically as a result of the positive and negative effects of CBM production. The experimental limitations and the characteristics of low permeability systems make it very difficult to measure the effective permeability of gas and water in coal.

Presently, the most common relative permeability models include the Corey (1954) model, the Corey and Rathgens (1956) model, the Pirson (1958) model, the Brooks and Corey (1966) model, and the fractal model (He et al., 2000; Li, 2004; Zhou et al., 2007). Because the Corey model is the most prevalent in coal reservoir simulation software (such as FAST, CBM, and COMET3), and the fractal theory is most successfully applied in coal pore structure analysis (Yao et al., 2009), we chose the Corey model as the basic model and the fractal model as the contrastive model for our analysis. The Palmer and Mansoori (1996, 1998), which is widely used to reflect the positive and negative effects during CBM production, is chosen as the foundation model for the simulation of absolute permeability.

#### 4.1.1. Corey model

Corey (1954) calculated relative permeability using the capillary pressure curve. The relative permeability of gas/water at saturation $S_w$ is:

$$k_{rg}=\left[1-\left(\frac{S_w-S_{wr}}{1-S_{wr}-S_{gr}}\right)\right]^2\left[1-\left(\frac{S_w-S_{wr}}{1-S_{wr}}\right)^2\right] \tag{1}$$

$$k_{rw}=\left(\frac{S_w-S_{wr}}{1-S_{wr}}\right)^4 \tag{2}$$

where $k_{rg}$ is the relative permeability of gas (dimensionless); $k_{rw}$ is the relative permeability of water (dimensionless); $S_w$ is the water saturation fraction (dimensionless); $S_w$ is the irreducible water saturation fraction (dimensionless); and $S_{gr}$ is the residual gas saturation fraction (dimensionless).

### 4.1.2. The fractal model

Using the capillary pressure curve of rock, the fractal model for pore structure is established. This model calculates the gas and water relative permeabilities (He et al., 2000; Li, 2004; Zhou et al., 2007) using Eqs. (3) and (4):

$$k_{rg} = \left(1-\frac{S_w-S_{wr}-S_{gr}}{1-S_{wr}-S_{gr}}\right)^2\left(1-\left(\frac{S_w-S_{wr}}{1-S_{wr}}\right)^{\frac{5-D}{3-D}}\right) \tag{3}$$

$$k_{rw} = \left(\frac{S_w-S_{wr}}{1-S_{wr}}\right)^{\frac{11-3D}{3-D}} \tag{4}$$

where $D$ is the dimensionless fractal of seepage pores (pore radii larger than 100 nm).

The main lithotypes are semi-bright coals in study areas. The vitrinite reflectance ranges from 1.89% to 3.43%. Coal composition analysis shows that coals in this area are dominated by a maceral assemblage of vitrinite and subordinate inertinite. Proximate analysis indicates that the coals contain 0.09–0.40% moisture and 5.83–13.43% ash (Table 1).

In coal reservoirs, the fractal dimension of the seepage pores, which have the greatest contribution to the relative permeability, is usually calculated by mercury injection experiments (Pfeifer and Avnir, 1983). Our mercury injection experiments indicate that the average fractal dimension of the pore is 2.82 in Qinshui Basin (Table 2).

### 4.1.3. Palmer–Mansoori model

Palmer and Mansoori (1996, 1998) introduced a Levine (1996) adsorption model from the perspective of the strain effect. These authors regarded the matrix shrinkage effect as a function of pressure and proposed a permeability prediction model (PM model) in which uniaxial strain and constant vertical stress are assumed. The PM model is calculated by:

$$C_m = \frac{(1+v)(1-2v)}{E(1-v)} - \left[\frac{1+v}{3(1-v)}+f-1\right]\beta \tag{5}$$

$$\frac{k}{k_0} = \left[1+C_m\frac{(p-p)}{\phi_{fi}}+\frac{1}{3}\frac{S_{\max}}{\phi_{fi}}\left(\frac{1+v}{1-v}-3\right)\left(\frac{P}{P_L-P}-\frac{P_i}{P_L+P_i}\right)\right]^3 \tag{6}$$

where $E$ is Young's modulus (MPa); $v$ is Poisson's ratio; $\beta$ is the matrix compressibility ($\text{MPa}^{-1}$); $f$ is a fraction (0–1); $C_m$ is the coal compressibility ($\text{MPa}^{-1}$); $S_{\max}$ is the maximum Langmuir volumetric strain; $P_L$ is the Langmuir pressure (MPa); $P_i$ is the original reservoir pressure (MPa); $P$ is the current reservoir pressure (MPa); $k_0$ is the original reservoir permeability (mD); $k$ is the current reservoir permeability (mD); and $\phi_{fi}$ is the original reservoir porosity (dimensionless).

**Table 2**
Data of mercury injection experiments of cleats of coal samples (S1–S9) in the Qinshui basin.

| Sample number | S1 | S2 | S3 | S4 | S5 |
|---|---|---|---|---|---|
| Fractal dimension D | 2.8893 | 2.8730 | 2.4298 | 2.8736 | 2.7524 |
| Sample number | S6 | S7 | S8 | S9 | Average |
| Fractal dimension D | 2.7382 | 2.9905 | 2.9290 | 2.8971 | 2.8190 |

### 4.2. Model development

#### 4.2.1. Modeling reservoir pressure and water saturation

The production of coalbed methane is complex because a large amount of water can initially be produced from the cleats. Only after this phase is the pressure low enough for gas desorption to occur. With the decrease in water saturation, the reservoir fluid gradually transitions from a water single-phase into a gas and water two-phase. Therefore, during production, the reservoir pressure is closely related to the fluid saturation. The relationship between reservoir pressure and water saturation can be calculated using the CBM reservoir material balance equation (King, 1993).

At any time, the volume of cumulative gas production at surface conditions is equal to the following: the original free gas volume in the cleats + the original adsorption gas volume in the matrix – the residual free gas volume in the cleats – the residual adsorption gas volume in the matrix:

$$G_p = \frac{Ah\phi_{fi}(1-S_{wi})}{B_{gi}} + \rho_B AhV_L\frac{P_i}{P_i+P_L} - \frac{Ah\phi_{fi}\left(1-\bar{S}_w\right)}{B_{gi}} - \rho_B AhV_L\frac{P}{P+P_L} \tag{7}$$

where $G_p$ is the ground volume of the cumulative gas production at any time ($\text{m}^3$); $A$ is the gas supply area ($\text{m}^2$); $h$ is the thickness of the coal seam (m); $S_{wi}$ is the initial water saturation (dimensionless); $B_{gi}$ is the original gas volume coefficient ($\text{m}^3/\text{m}^3$); $\rho_B$ is the density of coal ($\text{kg/m}^3$); $\phi_f$ is the current porosity (dimensionless); $\bar{S}_w$ is the average water saturation (dimensionless); and $B_g$ is the current gas volume coefficient ($\text{m}^3/\text{m}^3$).

Additionally, the underground volume of water = the original water volume in the fracture + the increased water volume as a result of elastic expansion − the cumulative water production, as described in Eq. (8):

$$Ah\phi_f\bar{S}_w = Ah\phi_{fi}S_{wi} + Ah\phi_{fi}S_{wi}C_w(p_i-p) - W_pB_w \tag{8}$$

where $W_p$ is the ground volume of the cumulative water production at any time ($\text{m}^3$); $B_w$ is the water volume coefficient ($\text{m}^3/\text{m}^3$); and $C_w$ is the water compressibility ($\text{MPa}^{-1}$).

**Table 1**
Proximate and petrographic analysis of coal samples (S1–S9) in the Qinshui basin.

| Sample number | Coal mine | Coal seam | Coal lithotype | $R_{o,ran}$ (%) | Proximate analysis (%) | | | Coal composition (%) | | |
|---|---|---|---|---|---|---|---|---|---|---|
| | | | | | $M_{ad}$ | $A_{ad}$ | $V_{ad}$ | Vitrinite | Inertinite | Mineral |
| S1 | Sihe | 3 | Bright | 3.43 | 0.22 | 10.42 | 20.90 | 87.2 | 7.7 | 5.1 |
| S2 | Sihe | 3 | Semi-bright | 3.41 | 0.34 | 5.83 | 26.55 | 96.1 | 2.8 | 1.1 |
| S3 | Sihe | 3 | Bright | 3.20 | 0.29 | 13.43 | 6.08 | 90.6 | 1 | 8.4 |
| S4 | Sihe | 3 | Semi-bright | 2.84 | 0.22 | 8.16 | 6.04 | 86.3 | 10.3 | 3.4 |
| S5 | Jingfang | 3 | Semi-bright | 1.89 | 0.16 | 10.31 | 7.67 | 76.8 | 21.5 | 1.7 |
| S6 | Jingfang | 3 | Semi-bright | 1.93 | 0.40 | 12.87 | 6.74 | 65.7 | 33.6 | 0.7 |
| S7 | Jingfang | 3 | Semi-bright | 1.95 | 0.13 | 12.43 | 9.68 | 77.4 | 18.2 | 4.4 |
| S8 | Changcun | 3 | Semi-bright | 2.16 | 0.13 | 6.58 | 8.58 | 80.5 | 19.2 | 0.3 |
| S9 | Changcun | 3 | Semi-bright | 2.08 | 0.09 | 8.04 | 12.40 | 88.2 | 11 | 0.8 |

$M_{ad}$ = Moisture content (wt.%, air dry basis), $A_{ad}$ = Ash yield (wt.%, air dry basis), $V_{ad}$ = Volatile matter (wt.%, air dry basis).

The porosity changes under the positive and negative effects of production can be obtained from the PM equation:

$$\phi_f = \phi_{fi} - C_m(p_i - p) + \frac{S_{\max}}{3}\left(\frac{1+v}{1-v} - 3\right)\left(\frac{p}{p_L+p} - \frac{p_i}{p_L+p_i}\right) \tag{9}$$

followed by

$$\overline{S_w} = \frac{S_{wi}[1 + C_w(p_i - p)] - \dfrac{W_p B_w}{Ah\phi_{fi}}}{1 - \dfrac{C_m}{\phi_{fi}}(p_i - p) + \dfrac{S_{\max}}{3\phi_{fi}}\left(\dfrac{1+v}{1-v} - 3\right)\left(\dfrac{p}{p_L+p} - \dfrac{p_i}{p_L+p_i}\right)}. \tag{10}$$

Therefore, once a set of cumulative production values is obtained using the material balance equation, we can calculate the corresponding reservoir pressure. From the pressure, the corresponding average water saturation $\overline{S}_w$ is computed. However, because the material balance equation represents the gas and water two-phase seepage stage, the initial values of the model should correspond to the critical desorption pressure at the points when the production data are applied to the effective permeability model.

Using well1 with the data in Tables 3 and 4 as an example, a series of pressure and corresponding saturation values are computed by the material balance equation. Based on Fig. 4, the water saturation reductions under different initial water saturations are similar during the reservoir pressure decrease. A difference is that the lower the initial water saturation becomes, the lower the irreducible water saturation becomes.

#### 4.2.2. Modeling of porosity and irreducible water saturation

The porosity changes caused by the positive and negative effects of production could lead to changes in the irreducible water saturation. The mercury injection experiments for 9 coal samples from the Qinshui Basin indicate that the porosity of the samples is low while the irreducible water saturation is high (Table 5). The relationship between mercury injection porosity and irreducible water saturation (Fig. 5) can be expressed as:

$$y = 93.291e^{-0.065x}. \tag{11}$$

This equation can be used to predict the differences in irreducible water saturation associated with porosity changes.

#### 4.2.3. Endpoint relative permeability calibration

In contrast to a conventional petroleum reservoir, the endpoint relative permeability of a coal reservoir usually changes as a result of the positive and negative effects of production. Therefore, it is necessary to calibrate the endpoint relative permeability of coal reservoirs. We chose the water relative permeability at the maximum water saturation (100%) and the gas relative permeability at the irreducible water saturation, as measured by the steady-state method, as the endpoint values for calibration. This allows us to determine the flow law of gas and water in the coal reservoirs.

**Table 3**
Input data of well1 for material balance equation.

| Coal property | Acquisition approach | Value | Remark |
|---|---|---|---|
| $A(m^2)$ | Estimation | 31,400 | The experience value |
| $h(m)$ | Field data | 5 | |
| $\phi_{fi}$ | Experimental measurement | 0.03 | |
| $S_{wi}$ | Estimation | 1/0.9/0.8 | |
| $C_w(MPa^{-1})$ | References | 0.000464 | Seidle, 1999 |
| $C_m(MPa^{-1})$ | Experimental measurement | 0.000359 | |
| $B_{gi}(m^3/m^3)$ | Field data | 0.01 | |
| $\rho_B(kg/m^3)$ | Experimental measurement | 1600 | |
| $V_L(m^3/t)$ | Experimental measurement | 35 | Adsorption isothermal curve |
| $p_i(MPa)$ | Formula computation | 4.5 | |
| $p_L(MPa)$ | Experimental measurement | 3.2 | Adsorption isothermal curve |
| $B_w(m^3/m^3)$ | References | 1.0 | Qin and Li, 2006 |
| $v$ | Experimental measurement | 0.25 | |
| $S_{max}$ | Experimental measurement | 0.012 | |

**Table 4**
Data of cumulative gas/water production from well1 in the Qinshui basin for material balance equation.

| Production time t(a) | Cumulative gas production $G_p(m^3)$ | Cumulative water production $W_p(m^3)$ |
|---|---|---|
| 1 | 11778.00 | 497.70 |
| 1.5 | 141287.00 | 612.80 |
| 2 | 237148.00 | 632.95 |
| 2.5 | 333010.00 | 653.10 |
| 3 | 491227.00 | 718.50 |
| 3.5 | 569467.00 | 742.90 |
| 4 | 647707.00 | 767.30 |
| 4.5 | 762083.00 | 795.90 |
| 5 | 877655.00 | 813.60 |

#### 4.2.4. Effective permeability dynamic prediction model

Effective permeability is the most significant parameter for coalbed methane development. We considered the absolute permeability and relative permeability characteristics of the reservoirs and coupled these dynamic parameters with the material balance equation. After calibrating the endpoint relative permeability, an average gas and water effective permeability dynamic prediction model is established on the basis of the production data:

$$k_g = kk_{rg0}k_{rg} \tag{14}$$

$$k_w = kk_{rw0}k_{rw} \tag{15}$$

where $k_{rg0}$ is the endpoint relative permeability of gas (dimensionless); $k_{rw0}$ is the endpoint relative permeability of water (dimensionless); $k_g$ is the effective permeability of gas (mD); and $k_w$ is the effective permeability of water (mD).

## 5. Simulation results

### 5.1. Input parameters

Using the series of experiments described in Section 2 with the Qinshui coal samples, the partial parameters for the material balance equation and the permeability model are obtained. We collected production data for a typical production well in the Fanzhuang Block of the Qinshui Basin. The input parameters and production data are provided in Tables 6 and 7, respectively.

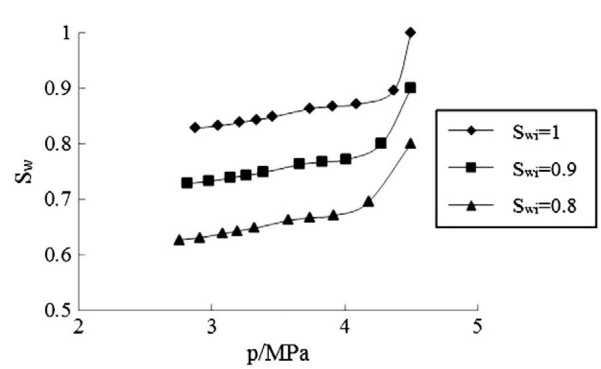


**Fig. 4.** The relationships between reservoir pressure (p) and water saturation ($S_w$) under different initial water saturation ($S_{wi}$).

**Table 5**
Data of mercury injection experiments of cleats of coal samples (S1–S9) in the Qinshui basin.

| Sample number | S1 | S2 | S3 | S4 | S5 | S6 | S7 | S8 | S9 |
|---|---|---|---|---|---|---|---|---|---|
| Porosity ϕ (%) | 6.1 | 4.6 | 4.5 | 3.2 | 3.1 | 2.7 | 2.3 | 2.0 | 1.7 |
| Irreducible water saturation $S_{wr}$ (%) | 63.73 | 66.12 | 72.60 | 73.40 | 76.91 | 75.06 | 79.30 | 83.20 | 86.8 |

### 5.2. Sensitivity analysis

Using the data in Tables 4 and 5, we plotted the effective permeability curves for the combination of the three basic models (Figs. 6 and 7). Fig. 6 indicates that the dynamic change in absolute permeability has an obvious influence on the gas effective permeability at low water saturation. When the water saturation is high (>80%), the effective permeability curves are almost coincident. Once the water saturation decreases to less than 80%, the gas effective permeability under the dynamic permeability gradually becomes higher than the constant permeability case at the same water saturation. This result verifies that the increase in the absolute permeability, which is caused by the positive effect, helps improve the gas effective permeability.

Fig. 7 indicates that, as the irreducible water saturation decreases, the gas effective permeability slowly increases, while the water effective permeability experiences little change. Eventually, the maximum gas effective permeability approaches a value that is unaffected by the changes in the irreducible water saturation. Thus, the positive effect during the CBM production can transform partially irreducible water into movable water, which contributes to water flow and limits the increase of the gas effective permeability. Meanwhile, the decrease in irreducible water saturation broadens the two-phase flow region and its duration.

### 5.3. Application to coal samples

The experimental data obtained with the steady-state method (Table 8) are used to plot the effective permeability curve. The comparisons of the experimental curve and the simulation curves (Fig. 8) indicate that when the fractal model is used as the basic model for relative permeability, the effective permeability curve for water declines faster than the curve of the Corey model. The gas effective permeability curve increases more slowly, and the equivalent effective permeability point appears earlier; thus, the curves display weak correspondence. However, when relative permeability is calculated with the Corey model, the curves are more similar, and the gas effective permeability eventually reaches a higher value. When the water saturation decreases to the irreducible water saturation, the effective permeability curves cease to change.

The analysis indicates that the relative permeability index of the fractal model is approximately 6–7 times larger than that of the Corey model, which leads to a sharp decline in the water effective permeability and an earlier appearance of the equivalent effective permeability point. However, the water saturation does not decrease suddenly during production; therefore, the error is larger for the fractal model. The conventional core used for the steady-state test may have failed to account for the positive effects of production, which could improve the effective permeability for gas. Therefore, the gas effective permeability of the actual reservoir is lower than that of the model. When the two models are compared, the PM–Corey model appears to provide relatively reasonable values.

Additionally, Shen et al. (2011) conducted effective permeability experiments in the laboratory using Lijiacun coal samples from the

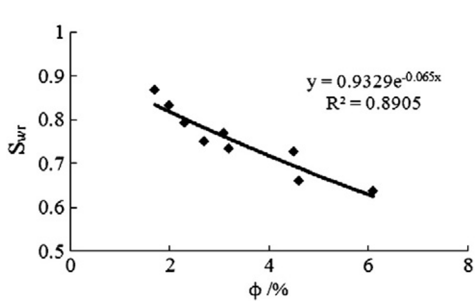


**Fig. 5.** Relationship of mercury injection porosity (ϕ) with irreducible water saturation ($S_{wr}$) of coal samples in the Qinshui basin.

**Table 6**
Input data for the gas and water effective permeability dynamic prediction model.

| Coal property | Acquisition approach | Value | Remark |
|---|---|---|---|
| $A(m^2)$ | Estimation | 31,400 | The experience value |
| $h(m)$ | Field data | 5.14 | |
| $\phi_{fi}$ | Experimental measurement | 0.04 | |
| $S_{wi}$ | Experimental measurement | 1 | |
| $B_{gi}(m^3/m^3)$ | Field data | 0.01 | |
| $\rho_B(kg/m^3)$ | Experimental measurement | 1600 | |
| $V_L(m^3/t)$ | Experimental measurement | 38 | Adsorption isothermal curve |
| $p_i(MPa)$ | Formula computation | 3.95 | |
| $p_L(MPa)$ | Experimental measurement | 3 | Adsorption isothermal curve |
| $B_w(m^3/m^3)$ | References | 1.0 | Qin and Li, 2006 |
| $W_p(m^3)$ | Production data | | Only for two-phase seepage stage |
| $G_p(m^3)$ | Production data | | Only for two-phase seepage stage |
| $C_w(MPa^{-1})$ | References | 0.000464 | Seidle, 1999 |
| $\nu$ | Experimental measurement | 0.25 | |
| $S_{max}$ | Experimental measurement | 0.012 | |
| $C_m(MPa^{-1})$ | Experimental measurement | 0.000359 | |
| $k_{rg0}$ | Experimental measurement | 0.756 | Relative permeability curve |
| $k_{rw0}$ | Experimental measurement | 1 | Relative permeability curve |
| $S_{wr}$ | Experimental measurement | 0.72 | Relative permeability curve |
| D | Experimental measurement | 2.82 | Mercury injection experiment |
| $S_{gr}$ | Estimation | 0.05 | |
| $\beta\ (MPa^{-1})$ | References | 0 | Palmer and Mansoori, 1998 |
| E(MPa) | Experimental measurement | 7000 | |
| $k_0(mD)$ | Experimental measurement | 0.585 | Measured with gas |
| f | References | 0.5 | Palmer and Mansoori, 1998 ranging from 0 to 1 |

**Table 7**
Data of cumulative gas/water production from CBM well in the Qinshui basin.

| Production time t(a) | Cumulative gas production $G_p(m^3)$ | Cumulative water production $W_p(m^3)$ |
|---|---|---|
| 1 | 144365.00 | 247.90 |
| 1.5 | 273193.00 | 398.20 |
| 2 | 497557.00 | 607.50 |
| 2.5 | 708605.00 | 808.00 |
| 3 | 926681.00 | 927.20 |
| 3.5 | 1161670.00 | 1010.90 |
| 4 | 1427170.00 | 1131.30 |
| 4.5 | 1706350.00 | 1284.10 |
| 5 | 1994120.00 | 1367.30 |

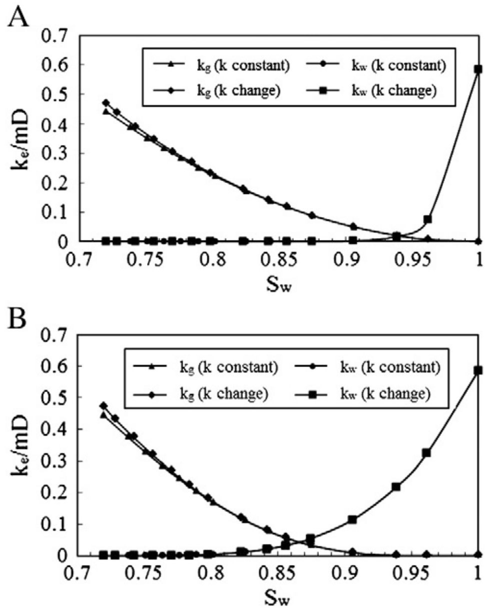


**Fig. 6.** Comparison of effective permeability ($k_e$) curves under different absolute permeability (k), A is PM–fractal model and B is PM–Corey model ($k_g$ represents gas effective permeability, $k_w$ represents water effective permeability, $S_w$ represents water saturation).

Qinshui Basin. A comparison of the measured curve (Fig. 9) to the PM–Corey model simulation curve indicates that the equivalent effective permeability point appears earlier in the simulation, the effective permeability for gas increases faster and the effective permeability for water better matches the experimental results. However, the gas effective permeability expected from the simulation eventually reaches a higher value than the gas effective permeability actually measured through the experiments. The discrepancy of these results, as explained above, is caused by the inability of the experimental apparatus to simulate the coal matrix shrinkage effect and by the gas–water displacement method used to obtain the experimental data.

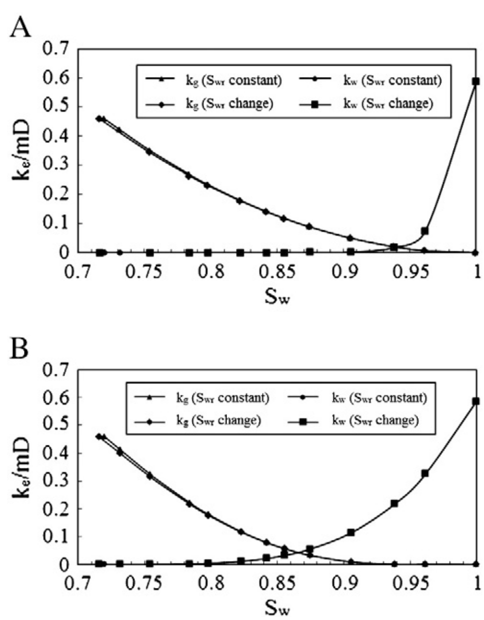


**Fig. 7.** Comparison of effective permeability ($k_e$) curves under different irreducible water saturation ($S_{wr}$), A is PM–fractal model and B is PM–Corey model ($k_g$ represents gas effective permeability, $k_w$ represents water effective permeability, $S_w$ represents water saturation).

**Table 8**
Data of relative permeability experiment by steady-state method.

| Water saturation | Relative permeability to gas | Relative permeability to water | Effective permeability to gas $k_g$(mD) | Effective permeability to water $k_w$(mD) |
|---|---|---|---|---|
| 1 | 0 | 1 | 0 | 0.585 |
| 0.97 | 0.008 | 0.386 | 0.005 | 0.225 |
| 0.96 | 0.041 | 0.305 | 0.024 | 0.178 |
| 0.94 | 0.053 | 0.264 | 0.031 | 0.154 |
| 0.92 | 0.072 | 0.212 | 0.042 | 0.124 |
| 0.90 | 0.092 | 0.163 | 0.054 | 0.095 |
| 0.86 | 0.131 | 0.113 | 0.077 | 0.066 |
| 0.82 | 0.177 | 0.076 | 0.103 | 0.044 |
| 0.78 | 0.272 | 0.038 | 0.159 | 0.022 |
| 0.75 | 0.335 | 0.022 | 0.196 | 0.013 |
| 0.73 | 0.441 | 0.013 | 0.258 | 0.0078 |
| 0.70 | 0.531 | 0.007 | 0.311 | 0.0041 |
| 0.68 | 0.694 | 0.005 | 0.406 | 0.0028 |
| 0.67 | 0.756 | 0.001 | 0.442 | 0.00041 |

## 6. Conclusions

1) The PM–Corey dynamic prediction model accurately reflects the positive and negative effects of coal reservoir production on the reservoir deliverability, especially the matrix shrinkage effect, which can improve the effective permeability of gas. Therefore, the model is feasible and can provide a basis for the analysis of production.
2) The material balance method can be used to calculate the average reservoir pressure and average water saturation. The changes in absolute permeability and relative permeability are obtained using these values. The regional average effective permeability dynamic prediction model is established through the simultaneous joining of the absolute permeability with the calibrated relative permeability.
3) The effective permeability is expressed as a unary function of the reservoir pressure, and the curve shape is controlled by the production data. By modifying the relative permeability models, we can calculate various effective permeability curves and choose the most appropriate one.
4) The PM–Corey dynamic prediction model more accurately reflects the positive and negative effects of coal reservoir production, especially the matrix shrinkage effect, which can improve the effective

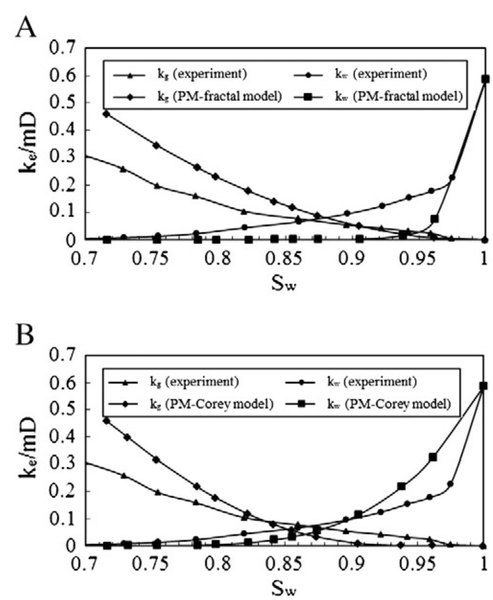


**Fig. 8.** Comparison of experimental and simulation effective permeability ($k_e$) curves, A is PM–fractal model and B is PM–Corey model ($k_g$ represents gas effective permeability, $k_w$ represents water effective permeability, $S_w$ represents water saturation).

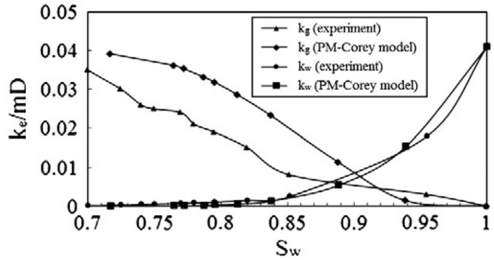


**Fig. 9.** Comparison of experimental effective permeability ($k_e$) curve (Shen et al., 2011) and PM–Corey model simulative curve ($k_g$ represents gas effective permeability, $k_w$ represents water effective permeability, $S_w$ represents water saturation).

permeability of gas. The dynamic changes in irreducible water extend the two-phase flow region.

## Acknowledgments

This work was financially supported by the National Natural Science Foundation of China (40730422), the Key Project of the National Science & Technology (2008ZX05034, 2009ZX05062), and the Fundamental Research Funds for the Central Universities (2011YXL052). The authors are grateful to the anonymous reviewers for their careful reviews and detailed comments. The authors also thank Prof. Shifeng Dai for his constructive suggestions and valuable assistance in the preparation of the manuscript.

## References

Ates, Y., Barron, Y., 1998. Effect of gas absorption on the strength of coal. Min. Sci. Technol. 6, 11–12.
Brooks, R.H., Corey, A.T., 1966. Properties of porous media affecting fluid flow. J. Irrig. Drain. Div. 6, 61.
Bustin, R.M., 1997. Importance of fabric and composition on the stress sensitivity of permeability in some coals, northern Sydney basin, Australia: relevance to coalbed methane exploration. AAPG Bull. 81, 1894–1908.
Cai, Y.D., Liu, D.M., Yao, Y.B., Li, J.Q., Qiu, Y.K., 2011. Geological controls on prediction of coalbed methane of No. 3 coal seam in Southern Qinshui Basin, North China. Int. J. Coal Geol. 88, 101–112.
Chen, Z.H., Wang, Y.B., Yang, J.S., Wang, X.H., Chen, Y.P., Zhao, Q.B., 2009. Influencing factors on coal bed methane production of single well: A case of Fanzhuang block in the south part of Qinshui basin. Acta Pet. Sin. 30, 409–416 (In Chinese with English abstract).
Chen, D., Pan, Z., Liu, J., Connell, L.D., 2013. An improved relative permeability model for coal reservoirs. Int. J. Coal Geol. 109–110, 45–57.
Clarkson, C.R., Jordan, C.L., Gierhart, R.R., Seidle, J.P., 2007. Production data analysis of CBM wells. Society of Petroleum Engineers paper 107705 presented at the SPE Rocky Mountain Oil and Gas Technology Symposium, Denver, CO.
Clarkson, C.R., Rahmanian, M., Kantzas, A., Morad, K., 2011. Relative permeability of CBM reservoirs: controls on curve shape. Int. J. Coal Geol. 88, 204–217.
Conway, M.J., Mavor, M.J., Saulsberry, J., Barree, R.B., Schraufnagel, R.A., 1995. Multi-phase Flow Properties for Coalbed Methane Wells: A Laboratory and Field Study. SPE Paper 29576.
Corey, A.T., 1954. The interrelation between gas and oil relative permeability. Prod. Mon. 31, 533–546.
Corey, A.T., Rathgens, C.H., 1956. Effect of stratification on relative permeability. Tech. Note 207, 358–360.
Cui, X., Bustin, R.M., 2005. Volumetric strain associated with methane desorption and its impact on coalbed gas production from deep coal seams. AAPG Bull. 89, 1181–1202.
Dai, S., Ren, D., Chou, C.-L., Finkelman, R.B., Seredin, V.V., Zhou, Y., 2012. Geochemistry of trace elements in Chinese coals: a review of abundances, genetic types, impacts on human health, and industrial utilization. Int. J. Coal Geol. 94, 3–21.
Friesen, W.I., Mikula, R.J., 1987. Fractal dimensions of coal particles. J. Colloid Interface Sci. 120, 263–271.
Friesen, W.I., Ogunsola, O.I., 1995. Mercury porosimetry of upgraded western Canadian coals. Fuel 74, 604–609.
Fu, X., Qin, Y., Zhang, W., Wei, C., Zhou, R., 2005. Fractal classification and natural classification of coal pore structure based on migration of coalbed methane. Chin. Sci. Bull. 50, 66–71.
GB/T 212–2008, 2008. Chinese National Standard. Coal, Proximate Analysis of Coal (in Chinese).
Ham, Y., Kantzas, A., 2008. Measurement of relative permeability of coal: approaches and limitations. Society of Petroleum Engineers paper 114994 Presented at the CIPC/SPE Gas Technology Symposium 2008 Joint Conference, Calgary, Alberta, Canada.
He, Y., Wu, Y.J., Wu, N.S., 2000. A new method for measuring the relative permeability quantitatively. Pet. Explor. Dev. 27, 66–68 (In Chinese with English abstract).
Hyman, L.A., Brugler, M.L., Daneshjou, D., Ohen, H.A., 1992. Advances in laboratory measurement techniques of relative permeability and capillary pressure for coal seams. Quart. Rev. Methane Coal Seams Technol. 9, 9–16.
ISO 7404.3-1994, 1994. Methods for the Petrographic Analysis of Bituminous Coal and Anthracite—Part 3: Method of Determining Maceral Group Composition.
ISO 7404.5-1994, 1994. Method for the Petrographic Analysis of Bituminous Coal and Anthracite—Part 5: Method of Determining Microscopically the Reflectance of Vitrinite. MOD.
Jones, A.H., Bell, G.J., Schraufnagel, R.A., 1988. A review of the physical and mechanical properties of coal with implications for coal-bed methane well completion and production. Geology and Coalbed Methane Resources of the Northern San Juan Basin, Corolado and New Moxico, Rocky Mountain Association of Geologists, Denver Colorado. 169–182.
King, G.R., 1993. Material balance techniques for coal-seam and devonian shale gas reservoirs with limited water influx. SPE Reserv. Eval. Eng. 8, 67–75.
Levine, J.R., 1996. Model study of the influence of matrix shrinkage on absolute permeability of coalbed reservoirs. Geol. Soc. 109, 197–212.
Li, K., 2004. Theoretical development of the Brooks–Corey capillary pressure model from fractal modeling of porous media. Proceedings of the SPE/DOE Fourteenth Symposium on Improved Oil Recovery held in Tulsa, Oklahoma, April 17–21. SPE 89429.
Li, K., 2010. More general capillary pressure and relative permeability models from fractal geometry. J. Contam. Hydrol. 111, 13–24.
Lv, Y.M., Tang, D.Z., Xu, H., Luo, H.H., 2012. Production characteristics and the key factors in high-rank coalbed methane fields: a case study on the Fanzhuang Block, Southern Qinshui Basin, China. Int. J. Coal Geol. 96–97, 93–108.
Mahamud, M., López, Ó., Pis, J.J., Pajares, J.A., 2003. Textural characterization of coals using fractal analysis. Fuel Process. Technol. 81, 127–142.
McKee, C.R., Bumb, A.C., Koenig, R.A., 1988. Stress dependent permeability and porosity of coal and other geologic formations. Soc. Pet. Eng. Form. Eval. 3, 81–91.
Moore, T.A., 2012. Coalbed methane: a review. Int. J. Coal Geol. 101, 36–81.
Palmer, I., 2009. Permeability changes in coal: analytical modeling. Int. J. Coal Geol. 77, 119–126.
Palmer, I., Mansoori, J., 1996. How permeability depends on stress and pore pressure in coalbeds, a new model. SPE Annual Technical Conference and Exhibition. Denver, Colorado.
Palmer, I., Mansoori, J., 1998. Permeability depends on stress and pore pressure in coalbeds, a new model. SPE Reserv. Eval. Eng. 1, 539–544.
Pan, Z., Connell, L.D., 2012. Modelling permeability for coal reservoirs: a review of analytical models and testing data. Int. J. Coal Geol. 92, 1–44.
Pan, Z., Connell, L.D., Camilleri, M., 2010. Laboratory characterisation of coal reservoir permeability for primary and enhanced coalbed methane recovery. Int. J. Coal Geol. 82, 252–261.
Paterson, L., Meany, K., Smyth, M., 1992. Measurements of relative permeability, absolute permeability and fracture geometry in coal. Coalbed Methane Symposium, pp. 19–21.
Pfeifer, P., Avnir, D., 1983. Chemistry in noninteger dimensions between two and three. I. Fractal theory and heterogeneous surfaces. J. Chem. Phys. 79, 3558–3565.
Pirson, S.J., 1958. Oil Reservoir Engineering. McGraw-Hill Book Co., New York.
Puri, R., Evanoff, J.C., Brugler, M.L., 1991. Measurement of coal cleat porosity and relative permeability characteristics. SPE Gas Technology Symposium, 21491, pp. 93–104.
Qin, J., Li, A., 2006. Petrophysics. China University of Petroleum Press, Dongying, Shandong 85–86 (in Chinese with English abstract).
Seidle, J.P., 1999. A Modified P/Z Method for Coal Wells. SPE Rocky Mountain Regional Meeting. Gillette, Wyoming.
Shen, J., Qin, Y., Wang, Geoff X., Fu, X.H., Wei, C.T., Lei, B., 2011. Relative permeabilities of gas and water for different rank coals. Int. J. Coal Geol. 86, 266–275.
Shi, J.Q., Durucan, S., Fujioka, M., 2008. A reservoir simulation study of $CO_2$ injection and $N_2$ flooding at the Ishikari coalfield $CO_2$ storage pilot project, Japan. Int. J. Greenh. Gas Control 2, 47–57.
Sparks, D.P., McLendon, T.H., Saulisberry, J.L., Lambert, S.W., 1995. The effects of stress on coalbed reservoir performance, Black Warrior Basin, USA. Annual Technical SPE Conference Proceedings, Dallas. Pap. Soc. Pet. Eng. 30743, 339–351.
Tao, S., Wang, Y.B., Tang, D.Z., Xu, H., Lv, Y.M., He, W., Li, S., 2012. Dynamic variation effects of coal permeability during the coalbed methane development process in the Qinshui Basin, China. Int. J. Coal Geol. 93, 16–22.
Wang, X.J., 2006. Influence of Coal Quality Factors on Seam Permeability Associated with Coalbed Methane Production, Faculty of Science. University of New South Wales, Sydney, Australia 338.
Wang, X.J., Ward, C.R., 2009. Experimental investigation of permeability changes with pressure depletion in relation to coal quality. 2009 International Coalbed Methane Symposium University of Alabama.
Wyllie, M.R.J., Gardner, G.H.F., 1958. The generalized Kozeny–Carman equations: its application to problems of multiphase flow in porous media: Part 2—a novel approach to problems of fluid flow. World Oil 146, 8–16.
Xu, H., Zhang, S.H., Leng, X., Tang, D.Z., Wang, M.S., 2005. Analysis of pore system model and physical property of coal reservoir in the Qinshui Basin. Chin. Sci. Bull. 50, 52–58.
Xu, H., Tang, D.Z., Liu, D.M., Tang, S.H., Yang, F., Chen, X.Z., He, W., Deng, C.M., 2012. Study on coalbed methane accumulation characteristics and favorable areas in the Binchang Area, southwestern Ordos Basin, China. Int. J. Coal Geol. 95, 1–11.
Yao, Y.B., Liu, D.M., Tang, D.Z., Tang, S.H., Huang, W.H., Liu, Z., Che, Y., 2009. Fractal characterization of seepage-pores of coals from China: an investigation on permeability of coals. Comput. Geosci. 35, 1159–1166.
Zhou, K., Zhang, Q., Wang, Q., Yan, Y., Li, N., 2007. Calculation of gas and water relative permeability by the fractal model. Nat. Gas Ind. 27, 88–89 (In Chinese with English abstract).